Analysis of Legged Landers for the Survivable Soft Landing of Instrument Payloads

ROBERT M. LAURENSON* AND RONALD A. MELLIERE†
McDonnell Douglas Astronautics Company—East, St Louis, Mo.
AND
JOHN R. MCGEHEE‡
NASA Langley Research Center, Hampton, Va.

Two methods of analysis were developed for legged planetary landers. These consist of a Large-Displacement Gear Analysis and a Landing Dynamics Analysis. The Large-Displacement Gear Analysis is employed to determine the large-displacement stroking behavior and energy absorption characteristics of a typical gear. The spatial landing dynamics of a legged lander is predicted through the Landing Dynamics Analysis. Effects of structural flexibility and elastic-plastic gear load characteristics on loads and motions of the lander are determined. Validation of the analytical techniques employed in the Landing Dynamics Analysis is accomplished through comparison of predicted results and experimental data obtained during a model test program.

Introduction

VEHICLES with legged-type landing systems have been used in the Surveyor and Apollo programs for accomplishing soft landings on the moon, and a legged-type landing system is being developed for the Viking Martian Lander. Important considerations in the design of such vehicles are the effect of structural elasticity on landing loads and vehicle landing stability and the energy absorption capabilities of the landing gear. This paper describes two independent methods of analysis, the Large-Displacement Gear Analysis and the Landing Dynamics Analysis. The former is for the design of a single landing gear, whereas landing loads and motions for the entire lander may be determined with the latter.

Previous analyses[1,2] have been developed to study the landing motions of legged landers; however, these analyses do not allow the simulation of a flexible body in conjunction with elastic-plastic gear characteristics and soil representations as available with the Landing Dynamics Analysis. The Large-Displacement Gear Analysis is unique in its capability to investigate the large-displacement stroking behavior of a landing gear.

The Large-Displacement Gear Analysis provides the capability for statically investigating the stroking behavior, energy absorption characteristics, and internal load distributions in the struts of a single landing gear through a nonlinear finite-element method. This analysis is a design tool to aid in the evaluation of a gear configuration independent of a landing dynamics investigation.

The Landing Dynamics Analysis allows prediction of the spatial landing motions of a legged lander idealized either as a rigid body or as a flexible body, as well as for the determination of landing loads and lander stability boundaries. Representation of the landing surface (soil) characteristics are included in the determination of the motions of a legged lander.

These two methods of analysis[3] have been programed for solution on the CDC 6600 computer. Examples of the results obtained with these two analyses are discussed, and the Landing Dynamics Analysis is validated by comparison of analytical results with experimental data.

General Configuration of Legged Landers

The general configuration of a typical legged lander is shown in Fig. 1. For the present analyses, the legged lander is composed of two basic components: the center-body structure and landing gears. The vehicle's scientific instrumentation, power supplies, terminal descent engines, controls, etc., are mounted on the center-body structure.

Two landing gear configurations, the inverted tripod and cantilever gears shown in Fig. 2, are considered in the methods of analysis. The main strut of both gears incorporates an energy absorption system. Drag struts may also include an energy absorption system, or for the inverted tripod gear, these struts may simply be frame members stabilizing the main strut.

Large-Displacement Gear Analysis

A modified incremental-stiffness, finite-element approach is employed in statically investigating the large-displacement (nonlinear) stroking behavior of either an inverted tripod or cantilever landing gear. This analysis is a useful tool for preliminary design of an individual landing gear. It can be used to predict energy absorption characteristics and internal load distribution in the gear as a function of gear stroke for many gear designs prior to conducting a comprehensive dynamic analysis.

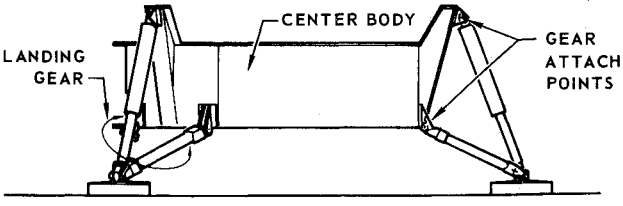

Fig. 1 Legged lander—general arrangement.

Presented as Paper 72-371 at the AIAA/ASME/SAE 13th Structures, Structural Dynamics, and Materials Conference, San Antonio, Texas, April 10–12, 1972; submitted May 4, 1972; revision received July 31, 1972. The methods of analysis described herein were developed as a part of Contract NAS 1-8137 for NASA. The model testing was conducted at NASA Langley Research Center. The authors wish to express their appreciation to the many individuals who contributed their efforts to the work described in this paper. Included are O. R. Otto (analysis) and R. L. Moore (programing) of McDonnell Douglas and S. M. Stubbs and U. J. Blanchard (model testing) of NASA Langley Research Center.

Index categories: Unmanned Lunar and Interplanetary Systems; Entry Vehicles Landers; Spacecraft Configurational and Structural Design (Including Loads).

* Group Engineer—Dynamics.
† Senior Engineer—Strength.
‡ Aerospace Technologist.

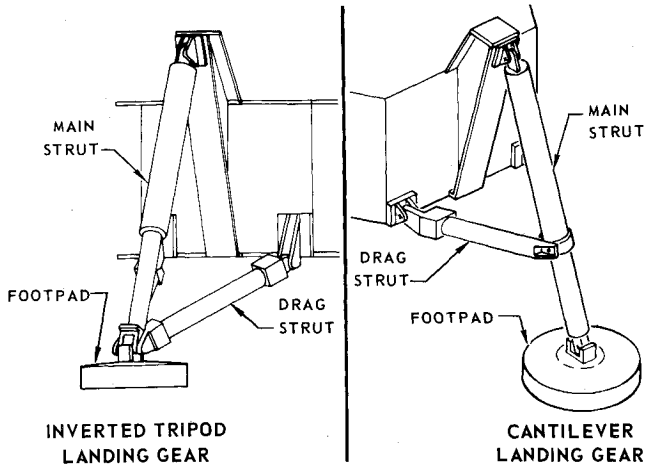

Fig. 2 Landing gear configurations.

An inverted tripod landing gear is idealized as three pin-ended elements representing the main strut and two drag struts. Four elements are used to idealize the cantilever landing gear. For this gear, the main strut is made up of two elements, both of which are capable of carrying bending as well as axial loads. These members are rigidly connected at the point where the drag struts join the main strut. The drag struts are represented as pin-ended axial load-carrying members. With the exception of the upper member of the cantilever gear main strut, all members in each type of gear may contain crushable material which attenuates loads in either tension or compression.

For struts containing crushable material, the strut is assumed to have an axial load-stroke curve for compression loading as shown in Fig. 3. This curve represents the stroking characteristics of stacked honeycomb cartridges housed within a landing gear strut. Each cartridge is assumed to crush at constant load as the strut is stroked. Cartridges possessing different crush levels may be stacked in series to form a desired load-stroke characteristic. For tension loading, similar load-stroke characteristics are assumed; however, the crush levels may be different than those for compression.

Referring to Fig. 3, typical strut loading as a function of stroke is as follows. As the strut initially begins to stroke, the strut load increases linearly with stroke to point 1 where the first crush load is reached. The load then remains constant with stroke until either the stroke reverses direction or a second elastic portion is reached. If the direction of stroke reverses, point 2, a number of load-stroke sequences, as indicated in Fig. 3, are possible. If at point 2 the stroke had not reversed direction, the load would continue to remain constant until point 7 was reached. The load would then increase linearly with stroke and continue to follow the load-stroke curve until unloading took place.

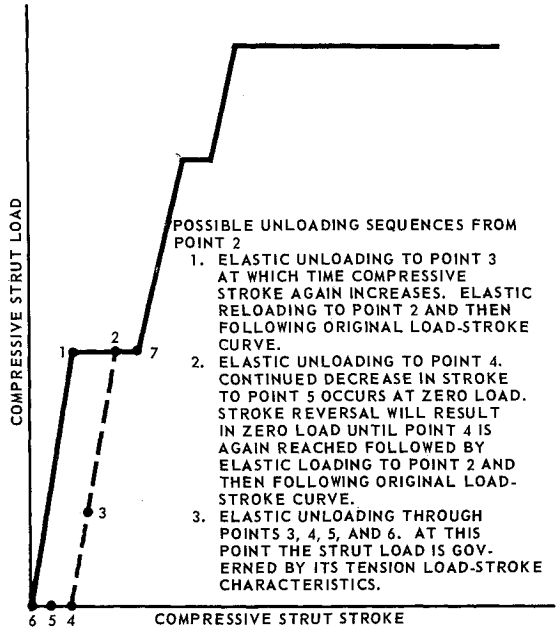

Fig. 3 Typical landing gear strut load stroke relationship.

Employing the finite-element idealization of the gear's struts described above, the spatial stiffness characteristics of the gear are formulated in terms of a stiffness matrix $[K]$. Thus gear loads $[F]$, and displacements $[\delta]$, are related through the expression

$$[F] = [K][\delta] \tag{1}$$

The stiffness matrix $[K]$ is the sum of the elastic stiffness $[K_e]$ and a geometric stiffness $[K_g]$.

$$[K] = [K_e] + [K_g] \tag{2}$$

The elastic stiffness, $[K_e]$, is dependent on the slope of each strut's load-stroke curve as well as on its spatial orientation and length. Hence, the contribution due to $[K_e]$ is zero for a strut containing crushable attenuation on a horizontal portion of the load-stroke curve (Fig. 3). The geometric stiffness, $[K_g]$, is a function of each strut's internal load, orientation, and length. Thus the contribution due to $[K_g]$ is not zero for a strut containing crushable attenuation even when on a horizontal portion of the load-stroke curve. Since both the elastic stiffness and geometric stiffness are a function of stroke, orientation, and length of each individual strut, the stiffness $[K]$ is a function of the gear's deformed shape and Eq. (1) is a nonlinear expression.

To illustrate the nonlinear nature of the problem, consider a planar gear subjected to the displacements shown in Fig. 4. Stiffness of the gear changes appreciably with deformation as evidenced by the changing slope of the load-stroke curve for the Y direction. This nonlinear behavior is approximated through a sequence of linear solutions. For instance, as indicated in Fig. 4, the total load in the Y direction has been divided into a number of equal increments (steps). The solution procedure in moving from load F_n to F_{n+1} is indicated on Fig. 5. Beginning at the deflected gear position, δ_n, corresponding to the applied load F_n, the increment of load $F_{n+1} - F_n$ is applied and the incremental displacements determined knowing the gear's stiffness, K_n, corresponding to the deformed shape δ_n. In the incremental-stiffness approach,[4] these displacements are added to the gear's position at the conclusion of the previous step to define the new deformed position. With this technique, the deformed position at the end of the step is defined by δ_A on Fig. 5.

Because of the linear approximations at each step of the incremental-stiffness technique, errors in the solution accumulate as a function of step size. This error is indicated by the difference between the applied load F_{n+1} and the internal load P_A corresponding to the deformation δ_A shown on Fig. 5. The modified incremental-stiffness method employs an iterative procedure to assure convergence to the correct solution and thus minimize this accumulation of errors.

In this technique the load unbalance, the difference between the applied load F_{n+1} and the internal load P_A, is applied to the structure whose incremental stiffness at the deformed shape δ_A is K_A. Thus, the new estimate of the gear's geometry is represented by δ_B and its corresponding incremental stiffness K_B. The internal load P_B is determined and the new load unbalance applied to the structure. This process is repeated, point C, until the load unbalance is arbitrarily small. When this occurs, the applied load is balanced by the internal load and equilibrium has been attained as indicated by point $n + 1$ and the resulting gear deformation δ_{n+1}.

To obtain the stroking characteristics of a gear for a given angular orientation of the gear relative to the landing surface, the landing surface is moved into the gear in a direction

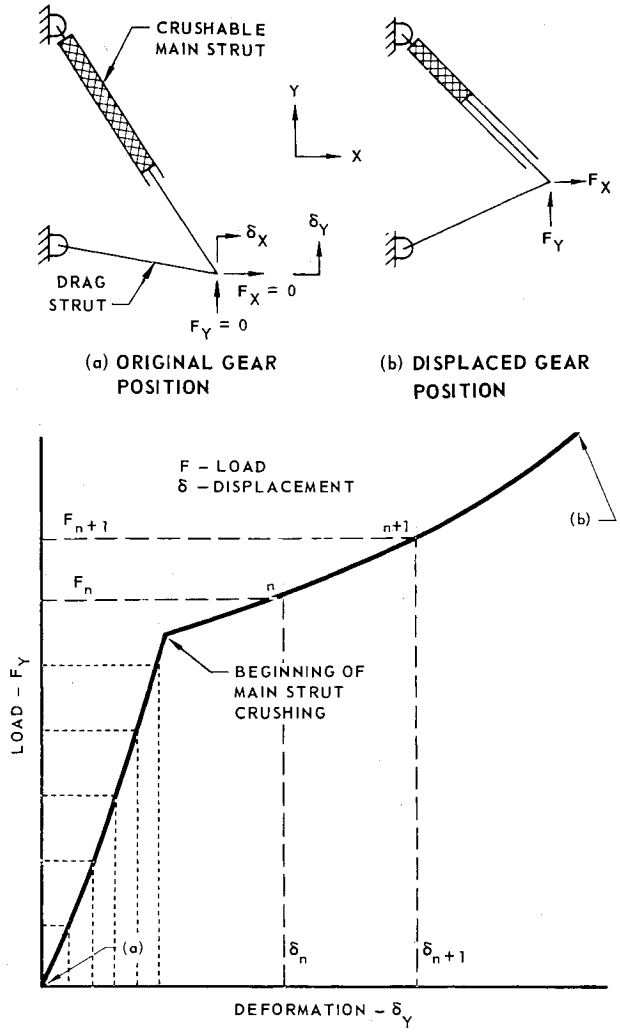

Fig. 4 Large-displacement behavior of a two-dimensional gear.

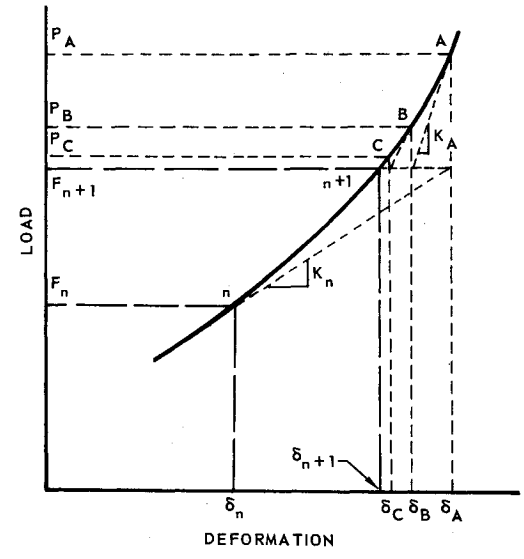

Fig. 5 Typical solution step for modified incremental-stiffness method.

normal to the surface and the resulting load-stroke relationship determined. In addition to the loads associated with the gear's stiffness properties, the effect of friction between the bottom of the footpad and the landing surface is included. This friction force is the force normal to the landing surface times the friction coefficient.

Of primary interest is the energy absorption capability of a landing gear configuration. Thus, the energy absorbed during each step of the gear's displacement history is determined. For each step this energy is expressed as the product of the average force over the step and the incremental displacement which occurred during the step. In addition, the energy contribution resulting from crushing of attenuation material at the bottom of the footpad may be included.

An example of the application of the Large-Displacement Gear Analysis is shown in Fig. 6. Here the $\frac{1}{6}$-scale Lunar Module cantilever gear[2] was analyzed to determine maximum energy absorption capability of the attenuation system as a function of landing surface orientation and friction coefficient. Various orientations of the landing surface, between 0° and 40°, were considered. Behavior of the gear was investigated by displacing the landing surface into the gear in a direction normal to the surface until the maximum allowable stroke was exceeded in one of the gear's struts. The energy absorbed by the attenuation system up to that point is the maximum energy absorption capability of the gear for that particular combination of landing surface orientation and friction coefficient. Results of this analysis are shown in Fig. 6. The difference in the energy absorption capability for the two values of surface friction is the result of the behavior of the footpad during stroking of the gear. For the lower friction, the footpad experiences significant sliding motion, whereas for friction coefficients of 0.8 and higher, the friction force was sufficient to prevent footpad sliding. As evidenced in Fig. 6, the gear's energy absorption capability is minimum for values of ground slope between 20° and 30°. At this orientation, motion of the surface relative to the gear is nearly colinear with the main strut, causing its allowable stroke to be exceeded before significant stroking of the drag struts occurs, regardless of friction coefficient.

Landing Dynamics Analysis

The Landing Dynamics Analysis provides techniques for the determination of spatial landing motions of a legged lander. For these motion predictions, the lander may be idealized either as a rigid body or as a flexible body. This analysis is unique

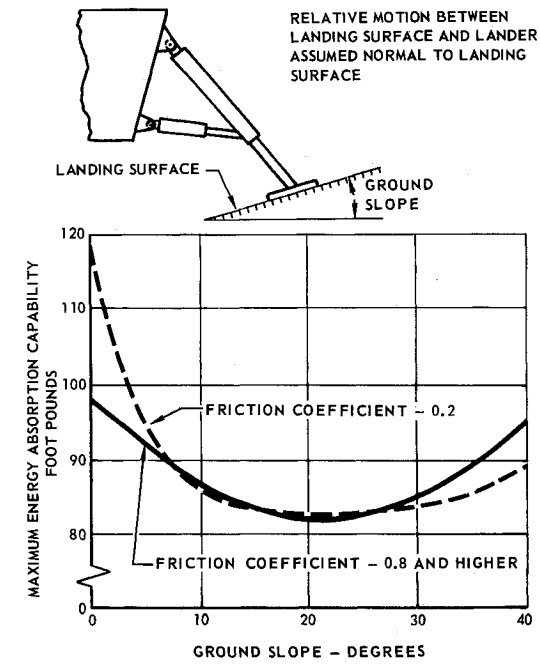

Fig. 6 Maximum energy absorption capability of a $\frac{1}{6}$-scale lunar module cantilever gear.

because of its capability for including not only landing gear elastic-plastic effects, but also the flexibility effects of the center-body structure on landing motions, loads, and stability.

When the lander's body is idealized as a rigid body, six equations of motion, including effects of large angular motions, are employed to completely define the lander's motion as a function of time. For investigating motions of a lander with a flexible center body, the normal mode method[5] is used. In this method, the elastic motion of the center body is approximated by the combination of a limited number of free-free vibratory modes. Total response is obtained by superimposing these resulting elastic deformations on the large-displacement rigid-body motions. Loads applied to the center body consist of the landing gear strut loads and gravitational loads.

Each footpad which is in contact with the landing surface is represented as a rigid mass having three translational degrees of freedom: one normal to the landing surface and two in the plane of the landing surface. The loads acting on a footpad are the landing gear strut loads, soil loads, and gravitational loads. When a footpad is not in contact with the landing surface these footpad equations of motion are not employed. Rather, the footpad is assumed to be an extension of the center-body structure, and its inertia effects are included in the solution of the center body's equations of motion.

An alternate procedure, in which a footpad's equation of motion are solved even if the footpad is not contacting the landing surface, is available. When a footpad is off the surface, loads applied to the footpad consist only of strut and gravitational loads. Thus, inertia loading of the landing gear struts due to the footpad mass may be simulated.

Two methods for representing the footpad-soil interaction are available. In the first method, empirical relationships defining the soil forces in terms of soil properties are used.[6] Soil properties required are the internal friction angle, relative density, and unit weight. Employing these soil parameters, empirical relationships are used to predict the soil forces as a function of footpad geometry, soil penetration, and velocity of penetration.

In the second method, the soil force normal to the footpad is determined in terms of depth of footpad penetration. This normal soil force is the product of the soil pressure and the area of the footpad projected on the landing surface. Initially, the soil pressure increases linearly from zero at zero penetration to a cutoff pressure at a specific depth. Beyond this depth, the soil pressure remains at the constant cutoff value. A force acting in the plane of the landing surface is obtained by multiplying the normal force by a selected coefficient of friction. This force is applied in a direction opposite to the footpad's velocity in the plane of the landing surface.

For a given lander configuration, either inverted tripod or cantilever gears may be considered. Each gear consists of a main strut and two drag struts which have pinned ends; thus, no moments or torques may be introduced at their ends. Each strut is capable of carrying elastic-plastic axial loads in either tension or compression. Representation of these elastic-plastic loads is similar to the techniques discussed in the Large-Displacement Gear Analysis, Fig. 3. For a cantilever gear, the effect of bending in the main strut is included by altering the energy absorption properties of the drag struts. In addition to these loads, each strut may have a load proportional to velocity and a constant load resulting from friction. Solution of the footpad and center-body equations of motion defines the relative motion between the ends of each landing gear strut. This relative motion is used to determine the stroke and stroking velocity of each strut.

Results from Landing Test Program

An experimental program has been conducted at the NASA Langley Research Center on models representing early versions of the Mars Viking legged lander having various landing gear configurations. Results obtained from a number of these experiments are compared with computed data to validate the Landing Dynamics Analysis.

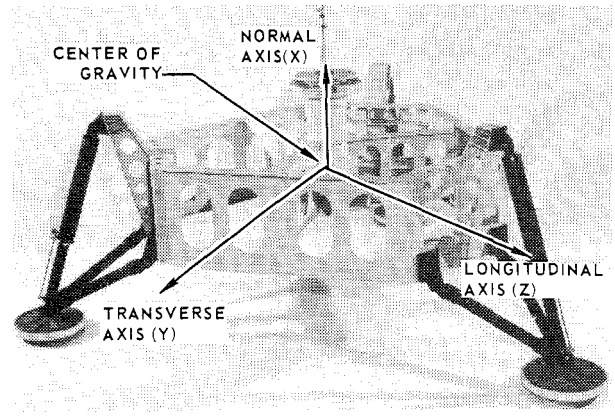

Fig. 7 Full-scale test model.

Description of Models

Two basic models of the Viking lander configuration were investigated in the experimental program: a full-scale model and a $\frac{3}{8}$-scale model. A photograph of the full-scale model is shown in Fig. 7. The landing gear is the inverted tripod configuration with energy absorption capability in the main struts and on the base of the footpads. The footpads are attached at the apex of the inverted tripod by universal joints which permit limited rotation about the longitudinal and transverse axes, but no rotation about the normal axis.

A photograph of one configuration of the $\frac{3}{8}$-scale model is shown in Fig. 8. This model, with the exception of the center-body structural design, is a $\frac{3}{8}$-scale version of the full-scale model shown in Fig. 7. The center-body structure, which consists of a stiff spaceframe structure internal to the gear attach points, was used to test three landing gear configurations. The gear configuration shown in Fig. 8 is an inverted tripod arrangement with only the main strut having energy absorption capability. A typical main strut, a four-stage crushable aluminum honeycomb element, and a two-stage footpad honeycomb element are shown. The drag struts are stiff tubular members.

The $\frac{3}{8}$-scale model was also tested with two other leg configurations, an inverted tripod with energy absorption capability in all struts and a cantilever gear. In this latter case, the $\frac{1}{6}$-scale Lunar Module gear[2] was employed. For both

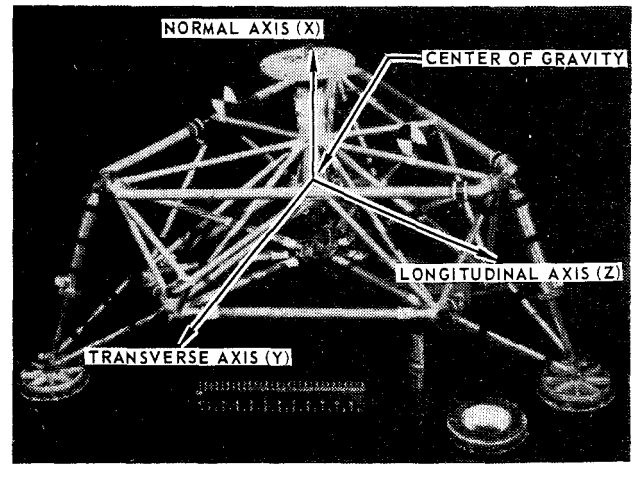

Fig. 8 $\frac{3}{8}$-scale test model.

configurations, the footpads were attached by ball joints to permit limited rotation of the pads about the longitudinal and transverse axes and unrestricted rotation about the normal axis.

All model configurations investigated were instrumented similarly. Normal, longitudinal, and transverse accelerations were measured at the c.g. of the models by piezoresistive strain-gage accelerometers. Strut strokes were measured on the main struts and drag struts, where applicable, by linear potentiometers. Strain gages were attached to all three struts of each landing gear and were calibrated to measure the force in each strut. The signals from the accelerometers, potentiometers, and strain gages were transmitted through trailing cables to FM tape recorders. In the process of data reduction, the acceleration and stroke data were passed through 300 Hz low-pass filters, and the force data were filtered by 880 Hz low-pass filters to eliminate undesirable high-frequency structural oscillations. The data were digitized using a sample rate of 2000 samples/sec and stored on tapes which were processed to obtain machine plots of the data.

Full-Scale Model Results

The full-scale model had a very flexible center-body structure, particularly for deformations in the *Y-Z* plane. For the model landing on a stiff (hard) landing surface, experimental and analytical time histories for normal and longitudinal center-of-gravity accelerations are compared in Fig. 9. Analytical data were obtained for both a rigid and flexible center-body structure.

To obtain the center-body flexibility data, a finite-element model of the center-body structure was developed. Using this model, a modal analysis was conducted to determine the center-body free-free frequencies and mode shapes. Three modes, with frequencies of 34.6, 48.2, and 101 Hz, were obtained whose modal deformation patterns were predominantly in the lander *Y-Z* plane and are of the type that would be excited by a landing such as that defined in the figure. These modes were included as input data for the Landing Dynamics Analysis when evaluating the effects of a flexible body.

As shown in Fig. 9, including flexibility effects results in better correlation between experimental and analytical acceleration data. The inclusion of center-body flexibility results in a less rapid buildup of acceleration upon impact, especially in the longitudinal direction. In addition, flexibility effects can readily be seen in the low-frequency oscillation present in the longitudinal acceleration.

There is some difference between the experimental and analytically predicted time-phasing of major events, such as the peak normal acceleration at approximately 0.035 sec. This may be attributed to slightly different values for the initial conditions employed in the analytical investigation as compared with those actually experienced in the test or differences between model structure and finite-element idealization. In spite of these differences, the agreement between experimental and analytical data is good.

A comparison between experimental and analytical load and stroke time histories for the main strut of the full-scale model is shown in Fig. 10. Touchdown parameters for the model, which were the same as those indicated on Fig. 9, resulted in two of the legs impacting the surface simultaneously, followed by impact of the third leg as the vehicle rotated in pitch. The force levels shown in Fig. 10 are well within the $\pm 10\%$ range from nominal levels obtained during dynamic crushing of typical strut honeycomb elements. The slightly greater analytical force levels would alter the impulse which would result in a change in the time phasing of subsequent leg-surface interactions. Data shown on this figure are typical of the good agreement obtained between experimental and analytical force and stroke data for all of the models investigated.

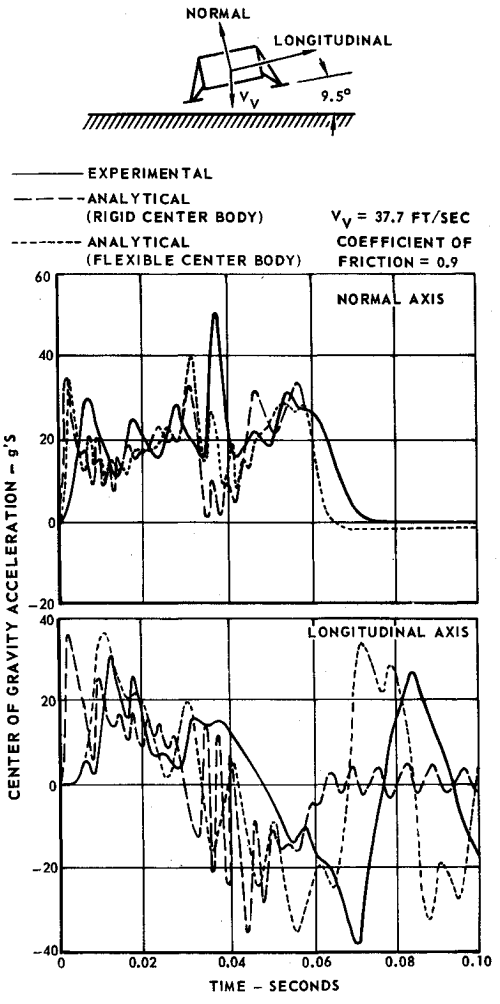

Fig. 9 Full-scale model acceleration time histories.

$\frac{3}{8}$-Scale Model Results

Accelerations in directions of principal motions were considered to be most inclusive of all of the parameters involved in a study of the landing motions of the various $\frac{3}{8}$-scale models tested. Consequently, the remaining comparisons of experimental and analytical data for the $\frac{3}{8}$-scale model will be made for accelerations along the model normal and longitudinal axes. Pertinent

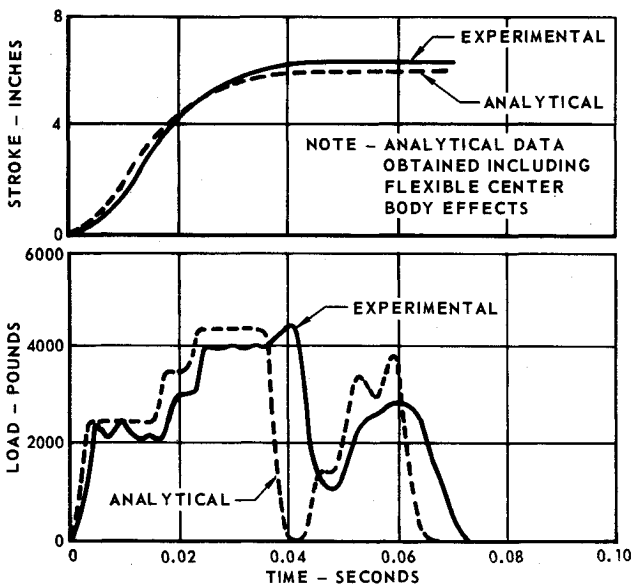

Fig. 10 Full-scale model main strut load and stroke time histories.

scaling relationships were employed to permit the $\frac{3}{8}$-scale model experimental data to be presented as full-scale data for a landing within the gravitational field of Mars. All analytical simulations were made for a full-scale vehicle landing on Mars. Due to the stiff tubular construction of the $\frac{3}{8}$-scale center body, the predicted motions were obtained assuming a rigid center body.

Experimental and analytical acceleration-time histories for the $\frac{3}{8}$-scale dynamic model with inverted tripod landing gear are presented in Fig. 11. Touchdown parameters resulted in the model impacting the landing surface with a single footpad. Rotational velocity generated during this impact resulted in the footpad leaving the surface and the model then rotating under free fall conditions. This was followed by impact of the two downhill footpads as indicated by the second set of acceleration pulses. The analytical data for the normal accelerations during the second pulse are lower than the average of those obtained from the experiment. This may be attributed to a small difference between the initial yaw angle input to the analytical investigation and that actually experienced during the experiment where the initial conditions were read from motion picture film.

Figure 12 presents comparisons between experimental and analytical acceleration time histories for the $\frac{3}{8}$-scale model with an inverted tripod leg configuration in which all struts contain energy absorbing honeycomb elements. The initial conditions resulted in almost simultaneous contact of all footpads with the landing surface and subsequent simultaneous loading of the leg struts. It was noted that the main struts for this gear configuration were susceptible to a stick-slip-type action. A constant friction force was included in the representation of the main strut characteristics to account for this phenomenon.

Normal and longitudinal acceleration time histories for experimental and analytical data obtained from a typical landing of the $\frac{3}{8}$-scale model with a cantilevered leg configuration are shown in Fig. 13. Loads applied to the main strut by the drag struts cause binding friction in the main strut. To represent this friction effect, which is particularly large early in the stroke when the stroking velocity is high, a main strut load proportional to the velocity cubed was included in the analysis.

Conclusions

Results obtained with the developed methods of analysis lead to the following conclusions. Flexibility of the lander center-body structure may significantly affect the landing dynamics of a legged lander. Load levels in struts for several of the landing gear configurations tested were found to include friction effects and the options available in the Landing Dynamics Analysis were capable of simulating these loads. Computations employing the Large-Displacement Gear Analysis indicated that landing gear orientation and landing surface friction greatly influence the large-displacement stroking behavior of a landing gear configuration.

Data obtained form the Landing Dynamics Analysis have been compared with experimental data for four lander configurations with various initial landing conditions. The agreement obtained between the experimental and analytical data is good for all of the lander configurations and touchdown parameters investigated. The basic Landing Dynamics Analysis, including vehicle structural elastic effects, has been shown to provide reliable predictions of the landing performance of legged-type lander vehicles.

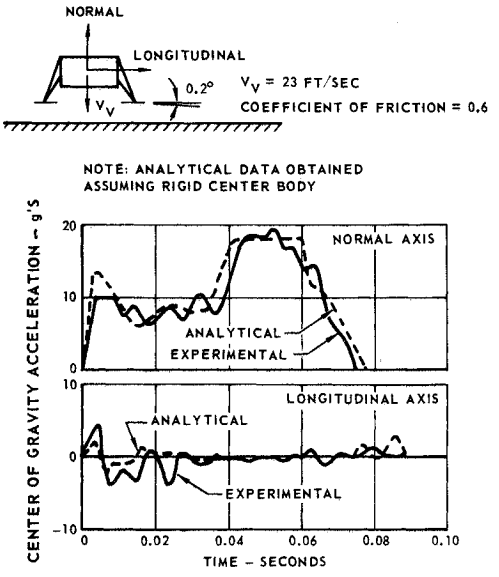

Fig. 12 Acceleration time histories for $\frac{3}{8}$-scale model with all crushable strut inverted tripod gears.

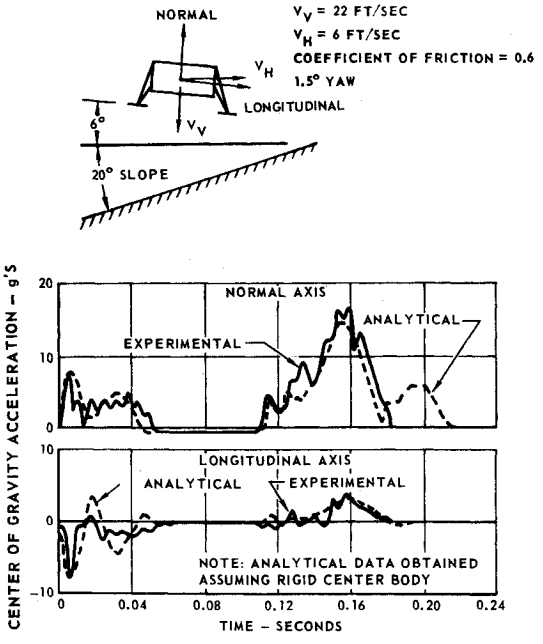

Fig. 11 Acceleration time histories for $\frac{3}{8}$-scale model with inverted tripod gears.

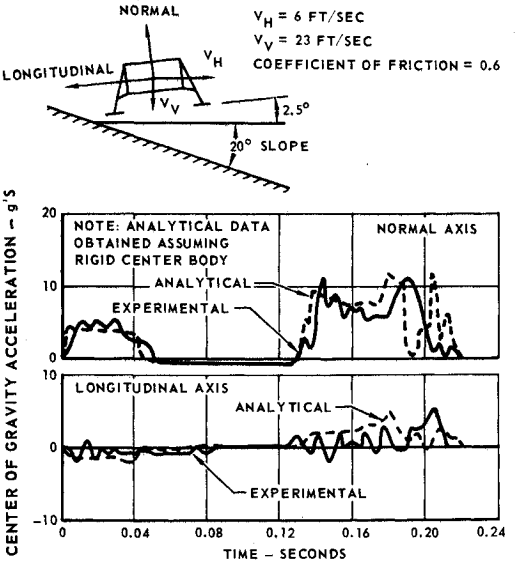

Fig. 13 Acceleration time histories for $\frac{3}{8}$-scale model with cantilever gears.

References

[1] Walton, W. C. and Durling, B. J., "A Procedure for Computing the Motion of a Lunar-Landing Vehicle during the Landing Impact," TN D-4216, Oct. 1967, NASA.

[2] Zupp, G. A., Jr. and Doiron, H. H., "A Mathematical Procedure for Predicting the Touchdown Dynamics of a Soft-Landing Vehicle," TN D-7045, Feb. 1971, NASA.

[3] Otto, O. R., Laurenson, R. M., Melliere, R. A., and Moore, R. L., "Analysis and Limited Evaluation of Payload and Legged Landing System Structures for the Survivable Soft Landing of Instrument Payloads," CR-111919, July 1971, NASA.

[4] Martin, H. C., "On the Derivation of Stiffness Matrices for the Analysis of Large Deflection and Stability Problems," *Proceedings of the Conference on Matrix Methods in Structural Mechanics*, TR-66-80, 1966, Wright-Patterson Air Force Base, Ohio.

[5] Bisplinghoff, R. L., Ashley, H., and Halfman, R. L., *Aeroelasticity*, Addison-Wesley, Cambridge, Mass., 1955, pp. 632–635.

[6] Anderson, R. G., "Application of LM Soil-Footpad Interaction Model to Surveyor Landing Dynamics Simulation," Paper 68K11, Nov. 1968, Bendix Energy Controls Div., South Bend, Ind.